# Optimized multibeam synthesis of time-modulated microstrip arrays

**Mudrik Alaydrus, Said Attamimi, Umaisaroh**
Department of Electrical Engineering, Faculty of Engineering, Universitas Mercu Buana, Jakarta, Indonesia

## Article Info

## ABSTRACT

The capability to form the main beam of antennas improves the energy efficiency of wireless systems and enhances radar systems' effectiveness in detecting and tracking objects. The time-modulated array can generate multibeam with arbitrary directions in different spectral parts. This work synthesizes several linear arrays to achieve particular main beams and additional restrictions. We modify the pulse durations and the switch-on instants of the switches in each antenna element in an optimization procedure. The parameters are varied through the simulated annealing by minimizing certain cost functions. We designed three linear arrays: model 1 consists of six elements and has two beams. Model 2 is the improved version of model 1 by rejecting the sidelobes of other spectral contributions at the main beam under consideration. Model 3 consists of sixteen elements and has three different beams. The analytical results were verified by modeling the arrays in the form of microstrip arrays in a numerical simulation with HFSS. We obtained very accurate verification. Distinctive devitations at the region $\vartheta < -60^o$ and $\vartheta > 60^o$ originate from the radiation characteristics of microstrip antennas, which focus the energy upwards to the region around $\vartheta = 0^o$.

*Corresponding Author:*

Mudrik Alaydrus
Department of Electrical Engineering, Faculty of Engineering, Universitas Mercu Buana
11650 Jakarta, Indonesia
Email: mudrikalaydrus@mercubuana.ac.id

## 1. INTRODUCTION

The advanced wireless communication systems promise several key performance indicators, such as higher data rate, low energy consumption, and higher spectral efficiency [1], which can be achieved by implementing beamforming capability in the transmitters and receivers. In radar applications, antennas with specific radiation patterns with beamforming are required [2] to ensure the radar performance to detect and track objects accurately. In [3], an antenna array consisting of four circularly polarized slotted elements was designed. Each antenna is connected to a radio frequency amplifier and a radio frequency phase shifter. In this way, the complex current distribution fed to each antenna can be adjusted to guarantee the correct beamforming. Moreover, using this approach, there are many possible errors, which degrade the quality of the beamforming in its sidelobe rejection and main lobe direction [4].

Yang et al. used low-frequency switches in all the antenna elements; in this way, they got a time-modulated current excitation in the antenna elements [5]-[8]. Furthermore, they used the differential evolution (DE) method to optimize the switching duration to get a low sidelobe by rejecting the sideband radiation [5]. Bio-inspired optimization methods, the ant lion optimization (ALO) in [9]-[11] and grasshopper optimization algorithms (GOA) in [12]-[14], were implemented to minimize the sidelobe level in a symmetric linear array. They delivered better results compared to well-known optimization methods such as

particle swarm optimization (PSO) [15], [16], firefly algorithm (FA) [17], [18], and genetic algorithm (GA) [19], [20].

The grey wolf optimization (GWO) algorithm, another bio-inspired method based on the social hierarchy and hunting behavior of the grey wolves, was implemented to exploit the beamforming capability in linear arrays [21]. Here was shown that the performance of GWO outperforms the GA. A seagull optimization algorithm (SOA) was recently implemented to synthesis linear arrays to obtain radiation patterns with low sidelobe levels with and without zeros [22]. The SOA is a new optimization method based on the moving and attacking behaviors of the seagull in nature. Another probabilistic optimization method widely used is simulated annealing, for example, designing planar multiband antennas [23] and in detecting of faults in linear antenna arrays [24].

In this paper, we would like to design multibeam arrays based on the time-modulated array [25], [26]. The multibeam is constructed by exploiting the resulting signals at the fundamental, first harmonic, and second harmonic frequencies. In contrast to other publications, we apply the algorithm of simulated annealing for minimizing certain cost functions. In this way we obtain the pulse duration and the switch-on instant in each element. Moreover, these analytical results will be verified by implementing the arrays in the form of microstrip arrays in a numerical simulation with HFSS.

## 2.    METHOD
### 2.1.    Time-modulated array

Time-modulated array (TMA) is just a typical antenna array, but in each feeding line, we connect a switch to do a specific time variation for the complex current amplitude in each antenna [27] as given in Figure 1. Figure 1(a) shows a generic linear time-modulated array arranged along the $z$-axis. The electronic switches $g_n(t)$ should make the automatic beamforming possible. In order to keep the complexity of the practical implementation low, we restrict the time function of the switching-on and switching-off to a rectangular pulse function with a uniform period of $T_o$, as given in Figure 1(b).
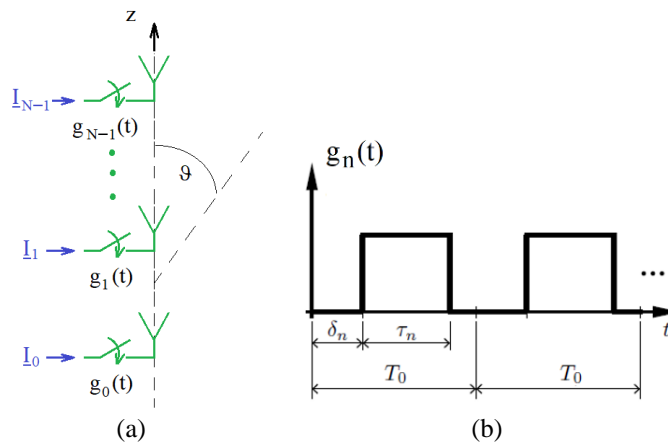


Figure 1. The principle of time-modulated array (a) TMA arrangement and (b) periodic rectangular pulse function of the switch

In this condition, the array factor of the linear TMA can be seen in (1),

$$AF(\vartheta, t) = e^{j2\pi f_c t} \sum_{n=0}^{N-1} g_n(t)\, \underline{I}_n\, e^{jkz_n \cos \vartheta} \tag{1}$$

$g_n(t)$ is a periodic rectangular pulse function with a period $T_o$, $\tau_n$ the pulse duration, and $\delta_n$ the switch-on instant. This periodic switching function can be described by expanding its Fourier series as shown in (2),

$$g_n(t) = \sum_{q=-\infty}^{+\infty} G_{nq}\, e^{j q \frac{2\pi}{T_o} t} \tag{2}$$

and especially for the periodic rectangular pulse function, the spectral contributions of all frequencies are given by:

$$G_{nq} = \xi_n \, \text{sinc}(q\pi\xi_n) \, e^{-jq\pi(\xi_n + 2o_n)} \tag{3}$$

where $\xi_n = \tau_n/T_o$ the normalized pulse duration and $o_n = \delta_n/T_o$ the normalized switch-on instant.

By inserting (2) and (3) into (1), we can represent the array factor of the TMA as a sum of two essential contributions

$$AF(\vartheta, t) = \underbrace{\left[\sum_{n=0}^{N-1} \underline{I}_n \xi_n e^{jkz_n \cos\vartheta}\right]}_{fundamental\ mode} e^{j2\pi f_c t}$$

$$+ \underbrace{\left[\sum_{n=0}^{N-1} \sum_{q=-\infty, q\neq 0}^{+\infty} \underline{I}_n \, \xi_n \, \text{sinc}(q\pi\xi_n) \, e^{-jq\pi(\xi_n + 2o_n)} \, e^{jkz_n \cos\vartheta}\right]}_{harmonics} e^{j2\pi(f_c + \frac{q}{T_o})t} \tag{4}$$

According to (4) is the most influential formulation of TMA. The array factor is split up into the fundamental mode and higher-order modes, so-called harmonics, representing sideband radiation (SR). As we can inspect from (4), if we feed the antenna elements with the same current $\underline{I}_n = \underline{I}_0$, the contribution of the fundamental mode is based only on the change in the new current contribution $\underline{I}_0 \xi_n$. In this way, we can only have the possibility to obtain a radiation pattern with a low sidelobe level (SLL). However, if we exploit the harmonics, we can enhance the beamsteering capabilities of the array through the new current contributions with $\underline{I}_0 \, \xi_n \, \text{sinc}(q\pi\xi_n)$ for the amplitude and $-q\pi(\xi_n + 2o_n)$ for the phase. In this way, we have the possibility to generate additional beams in different directions as sideband radiation contributions.

## 2.2. Simulated annealing

How to adjust the switching parameters in all feeds to achieve specific radiation patterns is a kind of inverse problem. Therefore, solving the problems often involves optimization procedures. Although various methods are developed in finding of accurate and efficient meta-heuristic combinatorial optimization procedures, recent research hybridizes the conventional algorithms with machine learning approach [28].

The concept of simulated annealing originated from a physical and chemical process in metallurgy to obtain high-quality metals. The broad outline of the annealing process is as follows; at the beginning of the annealing process, a metallic structure is melted at a very high temperature, then cooled down slowly so that when the system reaches approximately the thermodynamic equilibrium, we have specific low-energetic crystalline formations. More precisely, in the beginning, at a relatively high temperature, the molecules in the melting metals are untidy. They are in a rapid moving condition; they move in a random way in all directions to achieve their appropriate states. During the cooling down process, the molecules become more ordered, they change their condition slowly, and the system approaches a frozen ground state at the temperature T=0. The process can be considered as an adiabatic thermodynamic process to the high-quality state with the lowest energy. Beginning with a too low initial temperature or cooling down the temperature too fast, the system may become quenched to form defects, or freeze out in metastable states. In metallurgy, the system is caught in a local minimum energy state [29].

The original Metropolis scheme began with a high initial temperature and a specific energy state E. This initial configuration is altered by keeping the temperature constant. The energy of the new proposed configuration may be more or lower than the previous ones. The system in metallurgy is locked in a locally low energy state. If the new configuration consumes less energy, the new configuration is automatically accepted. If the energy change is positive, the new configuration will be accepted with a probability given by the Boltzmann factor $e^{-\Delta E/T}$. This process is repeated until the temperature is decreased and the entire process is repeated until a frozen condition is obtained at T=0. By analogy, the application of this Monte Carlo method to combinatorial problems is straighforward [30].

The current state of the thermodynamic system in the annealing process is analogous to the current solution of the combinatorial problem, the energy equation for the thermodynamic system is analogous to the cost function of the optimization, and the ground state is analogous to the global minimum as the problem's target. The main challenge in implementing the algorithm is no obvious analogy for the temperature T concerning a free parameter in the combinatorial problem. Additionally, avoiding entrainment in local minima (quenching) is determined by how the annealing process is scheduled, i.a., the choice of initial temperature, the number of iterations to be conducted at each temperature, and how the temperature is reduced at each step as the cooling mechanism proceeds. Figure 2 depicts the flow chart of the simulated annealing for optimizing electromagnetic problems.

The temperature reduction function employed in this study is $T_i = T_0 \, \alpha^i$, with $T_0$=1000 as the initial temperature, $T_i$ denotes the temperature for step i, $\alpha$=0.997, and the end temperature $T_{END}$=0.0015.

In optimization, we define a cost function that usually must be minimized. In designing a TMA, some of the important goals are minimizing SLL at the fundamental mode and/or at the first harmonics, or minimizing the SR at the second and third harmonics, and so on (q=2, 3, ...).

An appropriate proposed cost function could be:

$$L = w_1 \sum_{i=1}^{N_1} SLL_{f_c} + w_2 \sum_{i=1}^{N_2} SLL_{f_c \pm f_0} + w_3 \sum_{i=1}^{N_3} SR_{f_c \pm q f_0} \tag{5}$$

$N_1$, $N_2$, and $N_3$ are the numbers of optimized SLLs/SRs at the fundamental frequencies, at the first harmonics, and at higher harmonics, respectively, whereby $w_1$, $w_2$, and $w_3$ are the weights for these cost contributions.
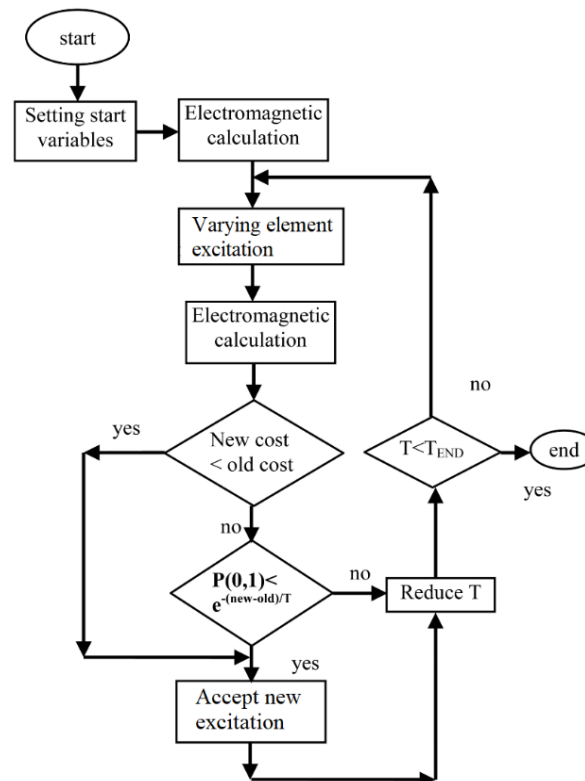


Figure 2. The algorithm of simulated annealing for optimizing the desired radiation pattern

## 3. RESULTS AND DISCUSSION

In this section we design several time-modulated arrays, which fulfill some prescribed characteristics. Simulated annealing optimization controls the design process by varying the pulse duration and the switch-on instant in each feeding. The optimization goal is to reduce the cost function given in (5). The obtained settings are then implemented in a commercial software package (HFSS) [31]. In this way, we verify the target radiation diagram of each model rigorously. The antenna elements are arranged along a line (one-dimensional array) and are separated at a distance of $0.5\lambda$.

### 3.1. Optimization-based design of time-modulated arrays
### 3.1.1. Time-modulated array with six elements

In model 1, we aim to get a main beam to the direction $\vartheta = 0^o$ at the fundamental frequency and another main beam to the direction $\vartheta = -30^o$ at the first harmonic frequency. As model 1, we propose an antenna with six elements that are separated equally by a distance of $\lambda/2$. With an initial start pulse duration and switch-on instant values, simulated annealing, according to the procedure as described in Figure 2, calculates the cost, which represents the deviations between the actual radiation diagram and the targeted ones. The optimization process continues by statistically varying the pulse duration and switch-on instant in each element. It ends if any stopping criterion is reached. Figure 3 summarizes the calculated result for model 1 after the simulation process. Figure 3(a) shows the optimized pulse duration and switch-on instant of the switch in each feeding line. We see that the pulse durations are around 0.5, which means around 50% of the antennas are on. The radiation diagram, as depicted in Figure 3(b), has a main beam at $\vartheta = 0^o$ at the

fundamental frequency (red line) and, at the same time, another main beam to $\vartheta = -30^o$ at the first harmonic frequency (blue line). By inspecting the sum of the Fourier components in each antenna, the contribution of the first harmonic compared to the fundamental frequencies is around 1.8759/3.2948=0.57, equal t $-4.9$ dB. On the other hand, the comparison of the second harmonic to the fundamental is around 0.2991/3.2948=0.09, equal to $-20.9$ dB, which can be considered as small, so can be neglected in this case.

In this model, we had as a target to obtain two main beams in directions $\vartheta = 0^o$ and $\vartheta = -30^o$. However, as we can see in Figure 3(b), there are a relatively high sidelobe of the first harmonic (around $-18$ dB) in the main direction of the fundamental mode ($\vartheta = 0^o$) and also a relatively high sidelobe of the fundamental mode (just around 9 dB below the main beam) in the main direction of the first harmonic ($\vartheta = -30^o$). This condition could pertube the communication link. In the following, we would like to improve this model by rejecting the sidelobe of the first harmonic frequency at $\vartheta = 0^o$ and the sidelobe of the fundamental frequency at $\vartheta = -30^o$, while maintaining the performance of the main lobes.

For these purposes, we modify the cost function by adding these additional targets. Figure 4 gives the result of the optimization process. In Figure 4(a), the switch-on duration of each antenna changes considerably. The central elements (#3 and #4) are switched on two times longer than the elements at the edges. The radiation diagram of the improved model, model 2, is given in Figure 4(b). We see that the sidelobe from the harmonic frequency at $\vartheta = 0^o$ reduced to more than $-30$ dB, and the sidelobe from the fundamental frequency at $\vartheta = -30^o$ reduced to $-35\ dB$. In both conditions, we have more than 30 dB isolation to prevent any possible interference. Moreover, we observe also due to energy reduction in these directions, we have an enhanced energy allocation to $\vartheta = -30^o$ at the main beam of the first harmonic frequency.
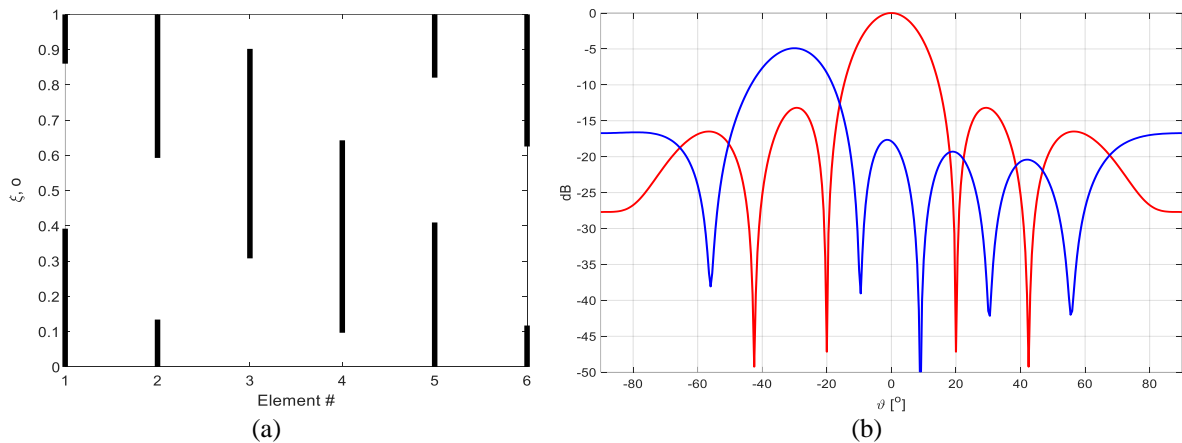


(a)                                        (b)

Figure 3. Result for model 1 (six elements) (a) optimized pulse duration ($\xi$) and switch-on instant ($o$) in each element and (b) radiation diagram at the fundamental frequency (red), first harmonic frequency (blue)
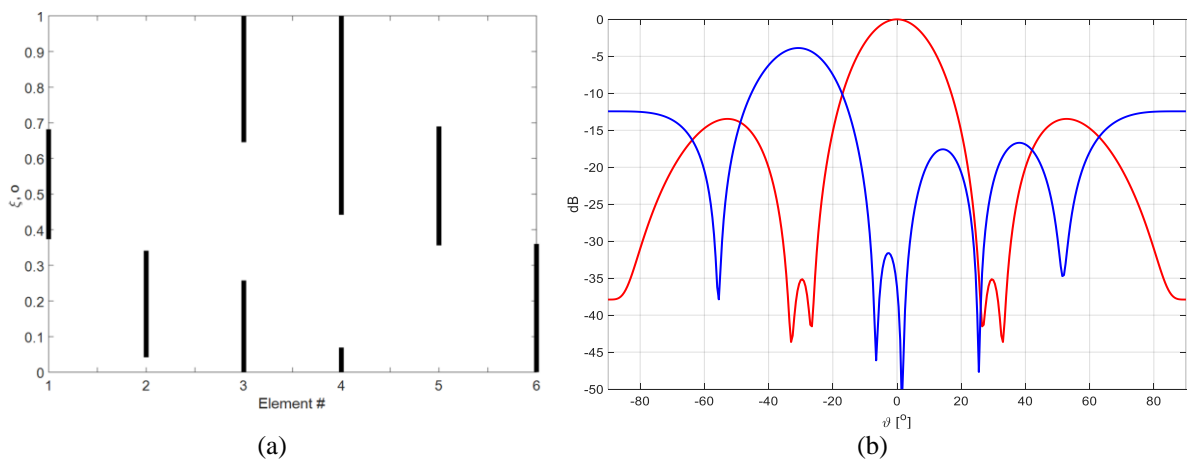


(a)                                        (b)

Figure 4. Result for model 2 (six elements (a) optimized pulse duration ($\xi$) and switch-on instant ($o$) in each element and (b) radiation diagram at the fundamental frequency (red), first harmonic frequency (blue)

In this model, by inspecting the sum of the fourier components in each antenna, the contribution of the first harmonic compared to the fundamental frequencies is around 1.6753/2.5412=0.66, equal to −3.6 dB. The comparison of the second harmonic to the fundamental is around 0.176/2.5412=0.07, equal to −23.9 dB, which again can be considered as negligible small.

### 3.1.2. Time-modulated array with sixteen elements

In model 3, we aim to get simultaneous beamforming to $\vartheta = 0^o, \vartheta = -45^o$, and $\vartheta = 35^o$ at the fundamental, first and second harmonic frequencies. At the same time, we require low signal level interference from each other. In order to fulfill these tight requirements, we propose an array with sixteen elements with equally spacing by $\lambda/2$. Figure 5 gives the pulse durations and the switch-on instants after the optimization process. We see, some elements are on in very short durations like elements #1, #2, #15 and #16 as compared to others which more active in use such as the elements in the middle part of the antenna, #6, #7, #8, #9, #10, #11.

The radiation diagram of these settings is given in Figure 6. We see, that the main beam at the fundamental frequency is oriented to $\vartheta = 0^o$, where the contributions of the first and second harmonic frequencies are lower than −40 dB. The main beam of the first and second harmonic frequencies is directed to $\vartheta = -45^o$ and $\vartheta = 35^o$, where the other spectral contributions are at around −40 dB. Overall, the possible interferers are lower than −30 dB than to the main beams. In this model, by inspecting the sum of the Fourier components in each antenna, the contribution of the first harmonic compared to the fundamental frequencies is around 2.9587/3.5=0.85, equal to −1.4 dB. The comparison of the second harmonic to the fundamental is around 1.7085/3.5=0.49, equal to −6.2 dB, as shown in Figure 6.
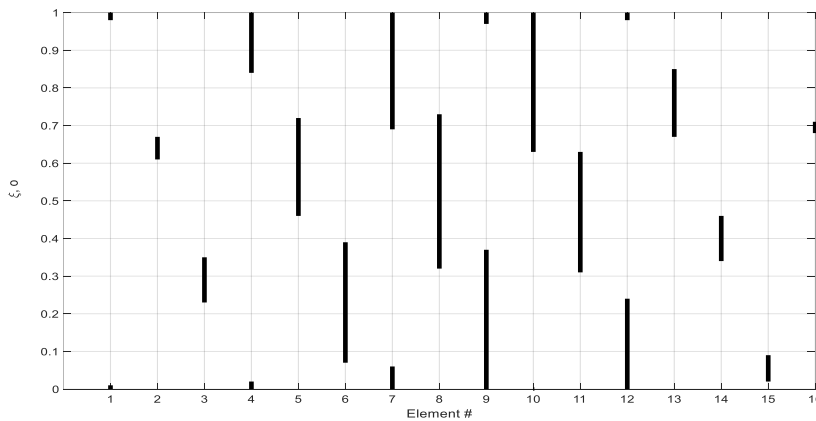


Figure 5. Optimized pulse duration ($\xi$) and switch-on instant ($o$) in each element of model 3 (16 elements)
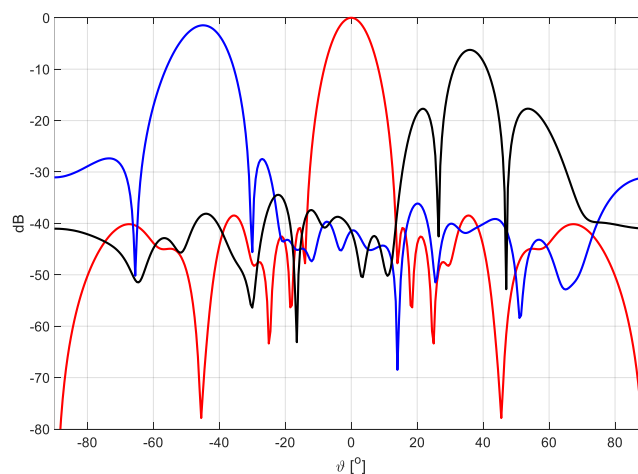


Figure 6. Radiation diagram of model 3 (sixteen elements), fundamental frequency (red), first harmonic frequency (blue), second harmonic frequency (black)

### 3.2. Numerical verification

In this section, we implement the designed array structures in microstrip technology and we calculate the radiation diagram numerically to verify the results obtained by the analytical approach described before. We use an FR4 substrate with a thickness of 1 mm, and we etch rectangular patches with a dimension of 11.6 mm x 11.6 cm, separated by a distance of 25 mm from each other. Figure 7 gives the computation model for the array with six and sixteen elements in HFSS. The antennas work at the mid-frequency of 5.8 GHz. The patches are fed by coaxial connectors from the ground side.
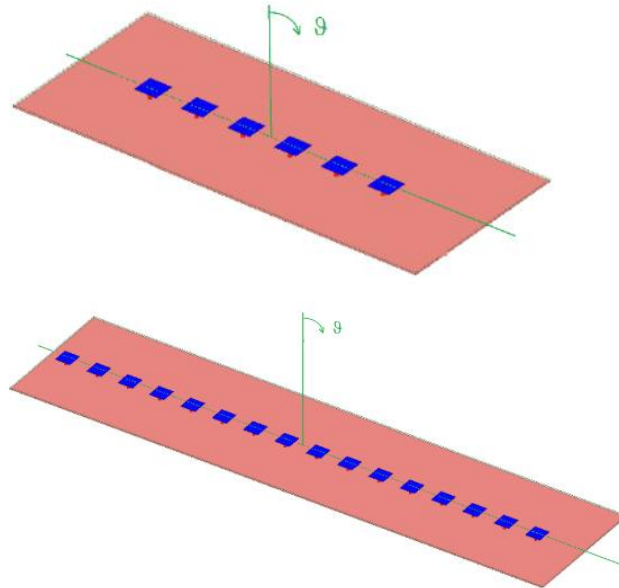


Figure 7. Models of Array with six and sixteen microstrip elements in HFSS

Figure 8 show comparisons between the results obtained in section 3.1, illustrated as solid lines, and the radiation diagrams calculated by HFSS, illustrated as dashed lines. Overall, the numerical calculations verify the analytical results, and we see the direction of the main beams, the signal levels, and the zero positions are reproduced accurately both for model 1 and model 2 as given in Figure 8(a) and (b), respectively. Distinctive devitations are observed at the region $\vartheta < -60^o$ and $\vartheta > 60^o$, which originate due to the radiation characteristics of microstrip antennas focusing the energy upwards to the region around $\vartheta = 0^o$ [32]-[34].



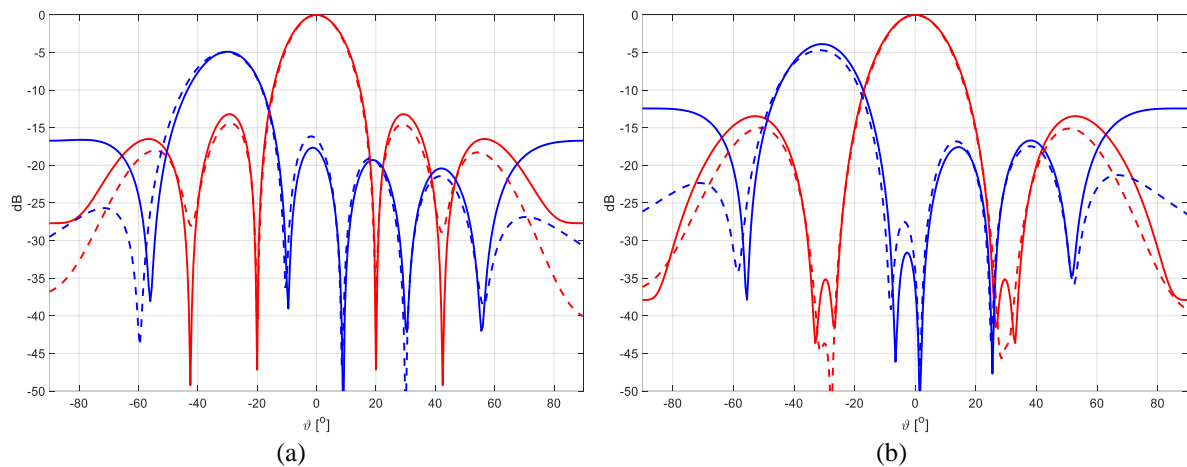(a)                                                      (b)

Figure 8. Comparison of radiation diagram obtained by optimization (solid lines) and its verification by HFSS (dashed lines) (a) model 1 and (b) model 2

*Optimized multibeam synthesis of time-modulated microstrip arrays (Mudrik Alaydrus)*

Figure 9 gives the comparison for model 3. Again, the numerical results verify the obtained analytical design very well. We see a very small shifting of the main beam for the first harmonic (blue curves) and for the second harmonic (black curves) by around 2º. And we see again some deviations at the edges of the observed radiation region ($\vartheta < -60^o$ and $\vartheta > 60^o$) due to the radiation characteristics of the microstrip antennas used in numerical simulations.
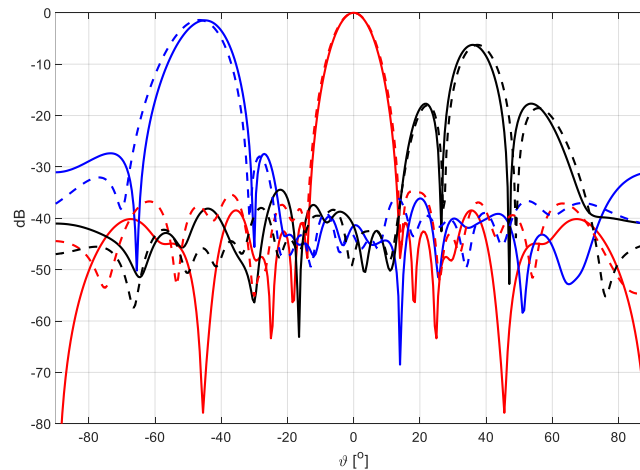


Figure 9. Comparison of radiation diagram obtained by optimization (solid lines) and its numerical verification by HFSS (dashed lines) of model 3 (sixteen elements), fundamental mode (red), first harmonic (blue), second harmonic (black)

## 4. CONCLUSION

In this work, we designed multibeam arrays based on the time-modulated array. The multibeam is contsructed by the fundamental, first harmonic, or second harmonic frequencies by varying the pulse duration and the switch-on instant in each element. These parameters are optimized through simulated annealing by minimizing the cost functions. We can show high-quality results and verify the radiation diagrams by numerical simulations with HFSS. Overall, the comparison of the obtained direction of the main beams, the signal levels, and the zero positions are very accurate. Distinctive devitations at the region $\vartheta < -60^o$ and $\vartheta > 60^o$ originate from the radiation characteristics of microstrip antennas, which focus the energy upwards to the region around $\vartheta = 0^o$.

## REFERENCES

[1]  B. Zheng, C. You, W. Mei, and R. Zhang, "A survey on channel estimation and practical passive beamforming design for intelligent reflecting surface aided wireless communications," *IEEE Communications Surveys and Tutorials*, vol. 24, no. 2, pp. 1035–1071, 2022, doi: 10.1109/COMST.2022.3155305.

[2]  Y. Yu, Z. H. Jiang, H. Zhang, Z. Zhang, and W. Hong, "A low-profile beamforming patch array with a cosecant fourth power pattern for millimeter-wave synthetic aperture radar applications," *IEEE Transactions on Antennas and Propagation*, vol. 68, no. 9, pp. 6486–6496, Sep. 2020, doi: 10.1109/TAP.2020.2999669.

[3]  M. Elhefnawy, "Design and simulation of an analog beamforming phased array antenna," *International Journal of Electrical and Computer Engineering (IJECE)*, vol. 10, no. 2, pp. 1398–1405, Apr. 2020, doi: 10.11591/ijece.v10i2.pp1398-1405.

[4]  H. Schrank, "Low sidelobe phased array antennas," *IEEE Antennas and Propagation Society Newsletter*, vol. 25, no. 2, pp. 4–9, 1983, doi: 10.1109/MAP.1983.27670.

[5]  S. Yang, Y. B. Gan, and A. Qing, "Sideband suppression in time-modulated linear arrays by the differential evolution algorithm," *IEEE Antennas and Wireless Propagation Letters*, vol. 1, pp. 173–175, 2002, doi: 10.1109/LAWP.2002.807789.

[6]  C. Shan, Y. Ma, H. Zhao, and J. Shi, "Time modulated array sideband suppression for joint radar-communications system based on the differential evolution algorithm," *Digital Signal Processing: A Review Journal*, vol. 97, Feb. 2020, doi: 10.1016/j.dsp.2019.102601.

[7]    W. Liang, R. Li, J. Li, and Z. Wu, "Modified differential evolution algorithm for time-modulated linear array antenna," *Applied Computational Electromagnetics Society Journal*, vol. 35, no. 10, pp. 1161–1168, Dec. 2020, doi: 10.47037/2020.ACES.J.351008.

[8]    S. Patra, S. K. Mandal, G. K. Mahanti, and N. Pathak, "Synthesis of unequally spaced time-modulated linear arrays through optimized position and on-time using differential evolution," in *Advances in Smart Communication Technology and Information Processing*, 2021, vol. 165, pp. 99–109, doi: 10.1007/978-981-15-9433-5_11.

[9]    A. A. Amaireh, A. S. Al-Zoubi, and N. I. Dib, "The optimal synthesis of scanned linear antenna arrays," *International Journal of Electrical and Computer Engineering (IJECE)*, vol. 10, no. 2, pp. 1477–1484, Apr. 2020, doi: 10.11591/ijece.v10i2.pp1477-1484.

[10]   P. Saxena and A. Kothari, "Ant Lion Optimization algorithm to control side lobe level and null depths in linear antenna arrays," *AEU - International Journal of Electronics and Communications*, vol. 70, no. 9, pp. 1339–1349, Sep. 2016, doi: 10.1016/j.aeue.2016.07.008.

[11]   H. Pradhan, B. B. Mangaraj, and S. K. Behera, "Chebyshev-based array for beam steering and null positioning using modified ant lion optimization," *International Journal of Microwave and Wireless Technologies*, vol. 14, no. 2, pp. 143–157, Mar. 2022, doi: 10.1017/S1759078721000295.

[12]   A. S. Al-Zoubi, A. A. Amaireh, and N. I. Dib, "Comparative and comprehensive study of linear antenna arrays' synthesis," *International Journal of Electrical and Computer Engineering (IJECE)*, vol. 12, no. 3, pp. 2645–2654, Jun. 2022, doi: 10.11591/ijece.v12i3.pp2645-2654.

[13]   H. Wang, C. Liu, H. Wu, B. Li, and X. Xie, "Optimal pattern synthesis of linear array and broadband design of whip antenna using grasshopper optimization algorithm," *International Journal of Antennas and Propagation*, vol. 2020, pp. 1–14, Jan. 2020, doi: 10.1155/2020/5904018.

[14]   Y. Meraihi, A. B. Gabis, S. Mirjalili, and A. Ramdane-Cherif, "Grasshopper optimization algorithm: theory, variants, and applications," *IEEE Access*, vol. 9, pp. 50001–50024, 2021, doi: 10.1109/ACCESS.2021.3067597.

[15]   J. R. Pérez and J. Basterrechea, "Hybrid particle swarm-based algorithms and their application to linear array synthesis," *Progress in Electromagnetics Research*, vol. 90, pp. 63–74, 2009, doi: 10.2528/pier08122212.

[16]   A. Durmus, R. Kurban, and E. Karakose, "A comparison of swarm-based optimization algorithms in linear antenna array synthesis," *Journal of Computational Electronics*, vol. 20, no. 4, pp. 1520–1531, Aug. 2021, doi: 10.1007/s10825-021-01711-w.

[17]   B. Basu and G. K. Mahanti, "Fire fly and artificial bees colony algo-rithm for synthesis of scanned and broad-side linear array antenna," *Progress In Electromagnetics Research B*, vol. 32, no. 32, pp. 169–190, 2011, doi: 10.2528/PIERB11053108.

[18]   A. Sharaqa and N. Dib, "Circular antenna array synthesis using firefly algorithm," *International Journal of RF and Microwave Computer-Aided Engineering*, vol. 24, no. 2, pp. 139–146, Mar. 2014, doi: 10.1002/mmce.20721.

[19]   D. Marcano and F. Durán, "Synthesis of antenna arrays using genetic algorithms," *IEEE Antennas and Propagation Magazine*, vol. 42, no. 3, pp. 12–20, Jun. 2000, doi: 10.1109/74.848944.

[20]   X. Yang, F. Yang, Y. Hong, Y. Ma, and S. Yang, "Synthesis of large-scale thinned arrays based on a multiagent genetic algorithm," *International Journal of RF and Microwave Computer-Aided Engineering*, vol. 31, no. 2, Feb. 2021, doi: 10.1002/mmce.22522.

[21]   A. I. Mohsin, A. S. Daghal, and A. H. Sallomi, "A beamforming study of the linear antenna array using grey Wolf optimization algorithm," *Indonesian Journal of Electrical Engineering and Computer Science (IJEECS)*, vol. 20, no. 3, pp. 1538–1546, Dec. 2020, doi: 10.11591/ijeecs.v20.i3.pp1538-1546.

[22]   E. Kurt, S. Basbug, and K. Guney, "Linear antenna array synthesis by modified seagull optimization algorithm," *Applied Computational Electromagnetics Society Journal*, vol. 36, no. 12, pp. 1552–1561, Mar. 2021, doi: 10.13052/2021.ACES.J.361206.

[23]   M. Alaydrus, "Planar antenna design controlled by simulated annealing," *Frequenz, vol.* 63, no. 7–8, pp. 139–143, Jan. 2009, doi: 10.1515/FREQ.2009.63.7-8.139.

[24]   N. Boopalan, A. K. Ramasamy, and F. H. Nagi, "Faulty antenna detection in a linear array using simulated annealing optimization," *Indonesian Journal of Electrical Engineering and Computer Science (IJEECS)*, vol. 19, no. 3, pp. 1340–1347, Sep. 2020, doi: 10.11591/ijeecs.v19.i3.pp1340-1347.

[25]   J. Tan, J. Hu, X. Dong, H. Li, and J. Zhou, "Research on pattern synthesis of time modulated sparse array based on discrete variable convex optimization," *Wireless Communications and Mobile Computing*, vol. 2021, pp. 1–12, Apr. 2021, doi: 10.1155/2021/6622168.

[26]   P. Rocca, F. Yang, L. Poli, and S. Yang, "Time-modulated array antennas–theory, techniques, and applications," *Journal of Electromagnetic Waves and Applications*, vol. 33, no. 12, pp. 1503–1531, Aug. 2019, doi: 10.1080/09205071.2019.1627251.

[27]   R. Maneiro-Catoira, J. Brégains, J. García-Naya, and L. Castedo, "Time modulated arrays: from their origin to their utilization in wireless communication systems," *Sensors*, vol. 17, no. 3, p. 590, Mar. 2017, doi: 10.3390/s17030590.

[28]   M. Karimi-Mamaghan, M. Mohammadi, P. Meyer, A. M. Karimi-Mamaghan, and E.-G. Talbi, "Machine learning at the service of meta-heuristics for solving combinatorial optimization problems: A state-of-the-art," *European Journal of Operational Research*, vol. 296, no. 2, pp. 393–422, Jan. 2022, doi: 10.1016/j.ejor.2021.04.032.

[29]   E. Aarts and E. Aarts, *Simulated Annealing and Boltzmann Machines: A Stochastic Approach to Combinatorial Optimization and Neural Computing*, Wiley, 1991.

[30]   W. Shao and G. Guo, "Multiple-try simulated annealing algorithm for global optimization," *Mathematical Problems in Engineering*, vol. 2018, pp. 1–11, Jul. 2018, doi: 10.1155/2018/9248318.

[31]   M. Wellandari, A. Firdausi, Umaisaroh, M. Alaydrus, "Design of hybrid element transmitarray antenna with beamforming at millimeter-wave frequency," *2021 International Conference on Radar, Antenna, Microwave, Electronics, and Telecommunications (ICRAMET)*, 2021. doi: 10.1109/ICRAMET53537.2021.9650461.

[32]   N. Ab Wahab, N. S. W. W. Muhamad, Z. I. Khan, and S. S. Sarnin, "Microstrip array antenna with inset-fed for WLAN application," *Indonesian Journal of Electrical Engineering and Computer Science (IJEECS)*, vol. 17, no. 1, pp. 340–346, Jan. 2019, doi: 10.11591/ijeecs.v17.i1.pp340-346.

[33]   S. M. Ali, V. Jeoti, T. Saeidi, and W. P. Wen, "Design of compact microstrip patch antenna for WBAN applications at ISM 2.4 GHz," *Indonesian Journal of Electrical Engineering and Computer Science (IJEECS)*, vol. 15, no. 3, pp. 1509–1516, Sep. 2019, doi: 10.11591/ijeecs.v15.i3.pp1509-1516.

[34]   V. Srinivasa Rao, K. V. V. S. Redd, and A. M. Prasad, "Bandwidth enhancement of metamaterial loaded microstrip antenna using double layered substrate," *Indonesian Journal of Electrical Engineering and Computer Science (IJEECS)*, vol. 5, no. 3, pp. 661–665, Mar. 2017, doi: 10.11591/ijeecs.v5.i3.pp661-665.

## BIOGRAPHIES OF AUTHORS

**Mudrik Alaydrus** received a Dr.-Ing. degree in Electrical Engineering from Universitaet Wuppertal. He is a professor at Universitas Mercu Buana, Jakarta. His current research includes microwave and millimeter-wave components, wireless power transfers, wireless sensor networks, and the interaction between electromagnetics and materials. He is a Senior Member of IEEE and member of Verein Deutscher Elektroingenieure (VDE) as well as member of Persatuan Insinyur Indonesia (PII). He can be contacted at email: mudrikalaydrus@mercubuana.ac.id.
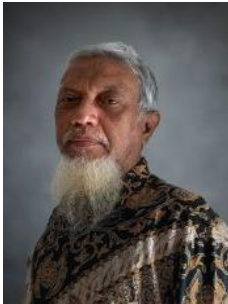
**Said Attamimi** is a senior lecturer at the Department of Electrical Engineering, Universitas Mercu Buana. He holds a bachelor's degree from Institut Teknologi Bandung and a master's degree from Universitas Indonesia, both in Electrical Engineering. He can be contacted at email: said@mercubuana.ac.id.

**Umaisaroh** is currently a lecturer with the Department of Electrical Engineering in Universitas Mercu Buana, Jakarta, Indonesia. She received the B.A.Sc. degree in Telecommunication Engineering from Politeknik Elektronika Negeri Surabaya (PENS), in 2013 and s Ph.D. degree in electrical engineering from Institut Teknologi Sepuluh Nopember (ITS), in 2019. She has been studied on HF skywave communications in equatorial regions. Her research interests include radio propagation, wireless communication, millimeter-wave, and antenna system. She can be contacted at email: umaisaroh@mercubuana.ac.id.